



MUSCLE DISEASE

Pathogenic *TNNI1* variants disrupt sarcomere contractility resulting in hypo- and hypercontractile muscle disease

Sandra Donkervoort^{1†}, Martijn van de Locht^{2†}, Dario Ronchi^{3‡}, Janine Reunert^{4‡}, Catriona A. McLean^{5,6‡}, Maha Zaki^{7‡}, Rotem Orbach¹, Josine M. de Winter², Stefan Conijn², Daan Hooimoed², Osorio Lopes Abath Neto^{1§}, Francesca Magri⁸, Angela N. Viaene⁹, A. Reghan Foley¹, Svetlana Gorokhova^{1,10,11}, Véronique Bolduc¹, Ying Hu¹, Nicole Acquaye¹, Laura Napoli¹², Julien H. Park¹³, Kalyan Immadisetty¹⁴, Lee B. Miles¹⁵, Mona Essawi¹⁶, Salar McModie¹⁷, Leonardo F. Ferreira^{2,18}, Simona Zanotti¹², Sarah B. Neuhaus¹, Livija Medne¹⁹, Nagham ElBagoury¹⁶, Kory R. Johnson²⁰, Yong Zhang²⁰, Nigel G. Laing^{21,22}, Mark R. Davis²¹, Robert J. Bryson-Richardson¹⁵, Darren T. Hwee²³, James J. Hartman²³, Fady I. Malik²³, Peter M. Kekenus-Huskey¹⁴, Giacomo Pietro Comi^{3,12¶}, Wessam Sharaf-Eldin^{16¶}, Thorsten Marquardt^{4¶}, Gianina Ravenscroft^{22¶}, Carsten G. Bönnemann^{1*#}, Coen A. C. Ottenheijm^{2*#}

Troponin I (TnI) regulates thin filament activation and muscle contraction. Two isoforms, TnI-fast (*TNNI2*) and TnI-slow (*TNNI1*), are predominantly expressed in fast- and slow-twitch myofibers, respectively. *TNNI2* variants are a rare cause of arthrogyriposis, whereas *TNNI1* variants have not been conclusively established to cause skeletal myopathy. We identified recessive loss-of-function *TNNI1* variants as well as dominant gain-of-function *TNNI1* variants as a cause of muscle disease, each with distinct physiological consequences and disease mechanisms. We identified three families with biallelic *TNNI1* variants (F1: p.R14H/c.190-9G>A, F2 and F3: homozygous p.R14C), resulting in loss of function, manifesting with early-onset progressive muscle weakness and rod formation on histology. We also identified two families with a dominantly acting heterozygous *TNNI1* variant (F4: p.R174Q and F5: p.K176del), resulting in gain of function, manifesting with muscle cramping, myalgias, and rod formation in F5. In zebrafish, TnI proteins with either of the missense variants (p.R14H; p.R174Q) incorporated into thin filaments. Molecular dynamics simulations suggested that the loss-of-function p.R14H variant decouples TnI from TnC, which was supported by functional studies showing a reduced force response of sarcomeres to submaximal [Ca²⁺] in patient myofibers. This contractile deficit could be reversed by a slow skeletal muscle troponin activator. In contrast, patient myofibers with the gain-of-function p.R174Q variant showed an increased force to submaximal [Ca²⁺], which was reversed by the small-molecule drug mavacamten. Our findings demonstrated that *TNNI1* variants can cause muscle disease with variant-specific pathomechanisms, manifesting as either a hypo- or a hypercontractile phenotype, suggesting rational therapeutic strategies for each mechanism.

INTRODUCTION

The troponin complex is critical for the regulation of muscle contraction [reviewed in (1)]. It is composed of three distinct subunits: a Ca²⁺ binding subunit (TnC), a tropomyosin binding subunit (TnT), and the actomyosin adenosine triphosphatase (ATPase) inhibitory

subunit (TnI). Upon muscle activation, Ca²⁺ enters the cytosol and binds to TnC, initiating a chain of events that leads to the release of TnI from actin, which allows movement of the tropomyosin dimer strand. This movement exposes myosin binding sites on actin and allows the myosin heads on the thick filament to grab and pull on the

¹Neuromuscular and Neurogenetic Disorders of Childhood Section, National Institute of Neurological Disorders and Stroke, National Institutes of Health, Bethesda, MD 20892, USA. ²Department of Physiology, Amsterdam UMC (location VUmc), Amsterdam, 1081 HV Netherlands. ³Dino Ferrari Center, Department of Pathophysiology and Transplantation, University of Milan, Milan, 20135, Italy. ⁴Department of General Pediatrics, University of Münster, Münster, 48149, Germany. ⁵Department of Anatomical Pathology, Alfred Hospital, Melbourne, Victoria, 3004, Australia. ⁶Faculty of Medicine, Nursing, and Health Sciences, Monash University, Melbourne, Victoria, 3168, Australia. ⁷Clinical Genetics Department, Human Genetics and Genome Research Institute, National Research Centre, Cairo, 12622, Egypt. ⁸Fondazione IRCCS Ca' Granda Ospedale Maggiore Policlinico, Neurology Unit, Milan, 20122, Italy. ⁹Department of Pathology and Laboratory Medicine, The Children's Hospital of Philadelphia, University of Pennsylvania Perelman School of Medicine, Philadelphia, 19104 PA, USA. ¹⁰Department of Medical Genetics, Timone Children's Hospital, APHM, Marseille, 13005, France. ¹¹INSERM, U1251-MMG, Aix-Marseille Université, Marseille, 13009, France. ¹²Fondazione IRCCS Ca' Granda Ospedale Maggiore Policlinico, Neuromuscular and Rare Disease Unit, Milan, 20122, Italy. ¹³Department of General Pediatrics, University Hospital Münster, Münster, 48149 Germany. ¹⁴Department of Cell and Molecular Physiology, Loyola University, Chicago, IL 60153, USA. ¹⁵School of Biological Sciences, Monash University, Melbourne, Victoria, 3800, Australia. ¹⁶Medical Molecular Genetics Department, Human Genetics and Genome Research Institute, National Research Centre, Cairo, 12622, Egypt. ¹⁷Department of Neurology, Alfred Health, Melbourne, Victoria, 3004, Australia. ¹⁸Department of Orthopaedic Surgery, Duke University School of Medicine, Durham, NC 27710, USA. ¹⁹Division of Human Genetics, Children's Hospital of Philadelphia, Philadelphia, PA 19104, USA. ²⁰Bioinformatics Core, National Institute of Neurological Disorders and Stroke, National Institutes of Health, Bethesda, MD 20892, USA. ²¹Neurogenetics Unit, Department of Diagnostic Genomics, PathWest Laboratory Medicine, QEII Medical Centre, Nedlands, Western Australia, 6009, Australia. ²²Centre for Medical Research University of Western Australia, Harry Perkins Institute of Medical Research, QEII Medical Centre, Nedlands, Western Australia, 6009, Australia. ²³Research and Development, Cytokinetics Inc., South San Francisco, CA 94080, USA.

*Corresponding author. Email: c.ottenheijm@amsterdamumc.nl (C.A.C.O.); bonnemanncg@nih.gov (C.G.B.)

†These authors contributed equally to this work.

‡These authors contributed equally to this work.

§Present address: Department of Pathology, University of Iowa Hospitals and Clinics, Iowa City, IA 52242, USA.

¶These authors contributed equally to this work.

#These authors contributed equally to this work.

actin molecules, thereby generating force along with the hydrolysis of adenosine triphosphate (ATP). With a decrease of cytosolic Ca^{2+} , TnI inhibits actomyosin ATPase, thereby regulating muscle relaxation. Thus, TnI plays an important role in skeletal muscle contraction and relaxation (1).

Genes encoding the Tn isoforms have been implicated in congenital (cardio)myopathies reviewed in (2), with the single exception of the gene encoding the slow skeletal TnI isoform [ssTnI; *TNNI1*; Online Mendelian Inheritance in Man (OMIM): 191042] (2). *TNNI1* was only recently tentatively implicated in myopathy in a single family with dominant proximal arthrogryposis, although the pathogenicity of the reported TnI variant (p.K175*) was not further investigated (3). ssTnI is predominantly expressed in fetal heart and slow-twitch skeletal myofibers (4, 5), whereas fast skeletal TnI (*TNNI2*) is expressed in fast-twitch skeletal myofibers and cTnI (*TNNI3*) is expressed in cardiac muscle. Variants in *TNNI2* (OMIM: 191043) are established causes of distal arthrogryposis syndromes (6, 7) and variants in *TNNI3* (OMIM: 191044) of cardiomyopathy (8).

Here, we characterized three independent families with biallelic loss-of-function *TNNI1* variants resulting in a hypocontractile phenotype, manifesting with early-onset progressive muscle weakness, as well as two families with dominantly acting heterozygous gain-of-function *TNNI1* variants resulting in a hypercontractile phenotype manifesting with muscle cramping and myalgia. Loss-of-function recessive variants caused hypotrophic myofibers with a reduced force response of the sarcomeres to submaximal $[\text{Ca}^{2+}]$, whereas the dominant variants caused hypertrophic myofibers with an increased force response of sarcomeres to submaximal $[\text{Ca}^{2+}]$ consistent with a gain-of-function hypercontractile manifestation. Thus, we established that pathogenic variants in *TNNI1* result in either a hypo- or a hypercontractile disease mechanism, which, for the hypocontractile mechanism, may be amendable to a troponin activator and, for the hypercontractile mechanism, may be amendable to the myosin inhibitor mavacamten.

RESULTS

Through exome- or next-generation-based sequencing (Supplementary Materials and Methods), we identified three families (F1: c.41G>A; p.R14H/c.190-9G>A, F2 and F3: homozygous c.40C>T; p.R14C), with biallelic recessive *TNNI1* variants and two families (F4: c.521G>A; p.R174Q and F5: c.527_529delAGA; p.K176del), with heterozygous dominant *TNNI1* variants. A summary of the identified *TNNI1* variants is shown in table S1. The positions of the variants in the protein molecule are indicated in Fig. 1A with its amino acid sequence around the variant in Fig. 1B. In general, the amino acid sequence of ssTnI is highly conserved across species (for example, 98% conservation between human and mouse *TNNI1*). The R14 residue is located in an α helix in the troponin C binding site. It is notable that R14 and its flanking sequences are conserved across all species queried. The dominant p.R174Q variant identified in F4 is located outside of known helices and binding sites of ssTnI but in a highly conserved region of the protein (Fig. 1B). In family 5, the c.527_529delAGA deletion in *TNNI1* was identified in the affected mother and her affected son. The variant likely results in the in-frame deletion of the residue lysine at codon 176 (p.K176del). Detailed clinical information for all patients is summarized in table S2.

Phenotype of loss-of-function recessive *TNNI1* variants

Family 1 (siblings: F1:P1 and F1:P2), family 2 (F2:P3), and family 3 (F3:P4) (Fig. 2A, left) presented with childhood onset myopathy

with proximal more than distal muscle weakness of moderate to severe clinical severity and progression. F2:P3 and F3:P4 presented with severe infantile weakness with minimal attainment of motor milestones. Visualization of muscle weakness is shown in Fig. 2B (left) (9). Respiratory involvement was variable, ranging from congenital onset need for mechanical ventilation (F2:P3) to a mildly reduced forced vital capacity (FVC) of 69% predicted (F1:P1). Both F1:P1 and F1:P2 had mild contractures of elbows, hamstrings, and heel cords. F2:P3 had moderate contractures of knees and hips in addition to bilateral hip dysplasia with subluxation of the left hip. F1:P2 was also noted to have rapidly progressive scoliosis, requiring surgery at age 13 years. F1:P1 was found to have an activity and load-induced tremor of low amplitude with high frequency that increased with weight-bearing activity or with persistent muscle use. None of the patients had a history of elevated serum creatine kinase (CK) levels. Echocardiogram screening was normal in all four affected individuals.

Phenotype of gain-of-function dominant *TNNI1* variants

Family 4 (three siblings F4:P5, F4:P6, and F4:P7) and family 5 (mother F5:P8 and son F5:P9) (Fig. 2A, right) presented with a dominantly inherited hypercontractile disease with a constellation of symptoms including muscle cramping, myalgias, stiffness, and fatigue, often after physical activity. Recognition of symptoms ranged from childhood (F4:P7) to adulthood (F5:P9) and was commonly reported as reduced exercise endurance and muscle cramping. Swallowing difficulties were present in four patients (F4:P5, F4:P6, F4:P7, and F5:P9). All patients were found to have elevated serum CK levels (ranging from 4 to 10 times upper limit of normal), typically preceding onset of clinical symptoms by years. Four of five patients reported normal muscle strength. F5:P8 developed progressive proximal lower extremity and axial [Medical Research Council (MRC) 4/5] weakness at age 64 years, which subsequently progressed to involve axial muscles and the upper extremity with mild biceps weakness (MRC 4+/5). Visualization of muscle weakness is shown in Fig. 2B (right) (9).

Respiratory surveillance (using FVC) and echocardiograms were normal in F4. The affected father in F4 passed away at age 66 years of sudden death. He had remained physically active and did not report muscle weakness. Echocardiogram in F5:P8 demonstrated mild left ventricular enlargement with a normal ejection fraction (67%). An electrocardiogram revealed nonspecific repolarization abnormalities at age 68 years. Her son (F5:P9) was diagnosed with mild left ventricular hypertrophy at age 43 years. At the age of 48 years, he was admitted for gastroenteritis and developed a myocarditis followed by cardiac arrest (asystole) requiring implantation of a pacemaker device. Cardiac magnetic resonance imaging (MRI) showed hypertrophic cardiomyopathy and acute myocarditis.

Muscle MRI findings

Muscle MRI of the lower extremities was performed in family 1 (F1:P1 and F1:P2) with recessive hypocontractile disease. In both siblings, there was a similar pattern of increased signal on T1-weighted images indicative of fatty changes within muscles, with relative sparing of the rectus femoris, gracilis, adductor longus, and semitendinosus muscles, along with the superficial vastus lateralis in F1:P1 in the upper leg and sparing of the medial and lateral gastrocnemius muscles in the lower leg (Fig. 2C, left). Among the affected muscles, muscles with a larger percentage of slow-twitch fibers, such as the soleus and vastus intermedius, showed more abnormal signaling. In the

Fig. 1. Slow skeletal troponin I protein (ssTnI) sequence and alignment. (A) Schematic representation of the amino acid sequence of ssTnI as encoded by *TNNI1* (FASTA: P19237). The recessive p.Arg14His (R14H) *TNNI1* substitution (family 1), p.Arg14Cys (R14C) (families 2 and 3), and the two dominant variants, p.Arg174Gln (R174Q) (family 4) and p.Lys176del (K176del) (family 5), are indicated. (B) Excerpts of cross-species *TNNI1* alignment in the regions of the patients' substitutions.

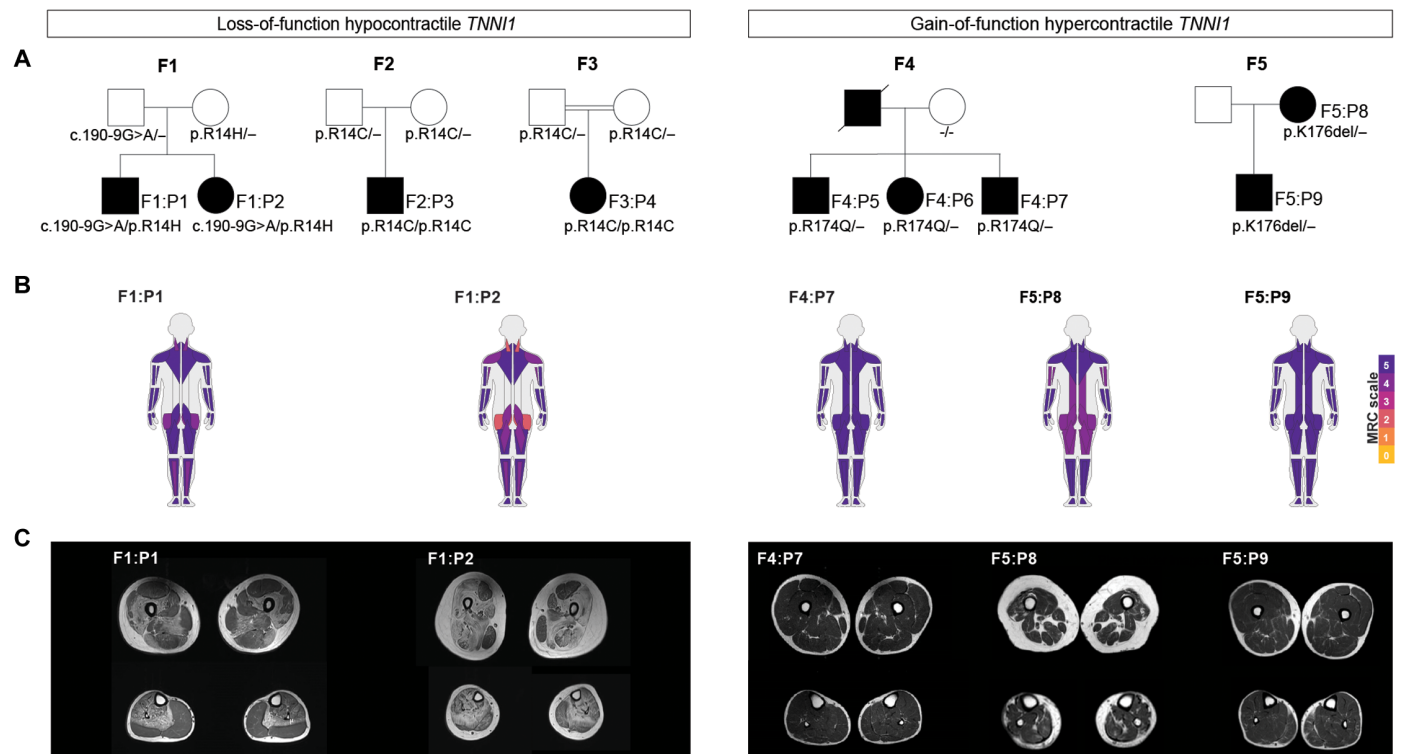
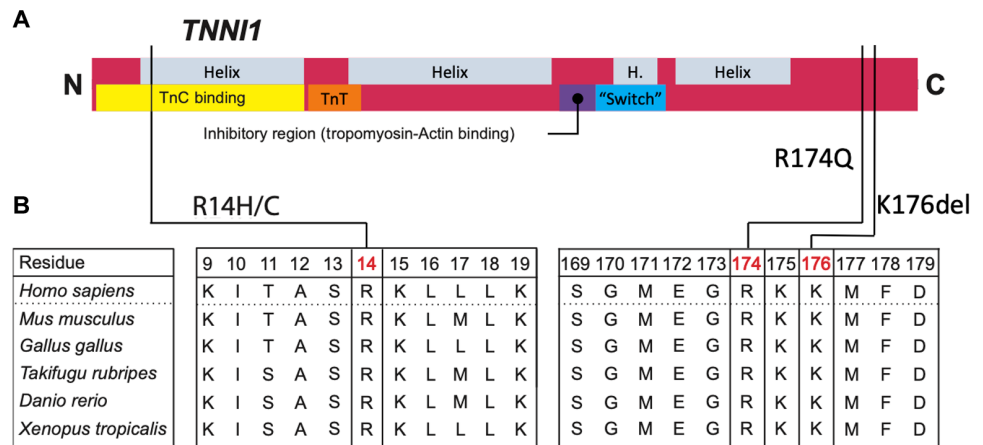


Fig. 2. Clinical and imaging characteristics of patients with *TNNI1* variants. (A) Pedigrees of the four families, with recessively inherited disease in families 1, 2, and 3 (left) and dominantly inherited disease in families 4 and 5 (right). (B) MuscleViz was used to visualize weakness using the MRC scale for muscle strength. (C) Left: Lower extremity muscle MRI imaging for patients F1:P1 and F1:P2 at age 18 and 15 years. Right: Lower extremity muscle MRI imaging for patients F4:P7, F5:P9, and F5:P8.

families with hypercontractile dominant disease (F4 and F5) muscle MRI revealed a distinct spectrum of involvement, ranging from normal appearance (F4:P7) to near-normal appearance with selective fatty infiltration of the medial gastrocnemius (F5:P9) and to mildly diffuse fatty infiltration without a specific pattern (F5:P8) (Fig. 2C, right). Overall, when compared with the recessive patients, the patients with dominant disease were found to have less pronounced signal changes indicative of fatty infiltration and without obvious atrophy.

Histological and ultrastructural findings

Muscle biopsies were obtained in three patients (F1:P1, F1:P2, and F2:P3) with hypocontractile *TNNI1* disease. Histological findings were consistent with a myopathic process in all three, with variability in fiber size on hematoxylin and eosin (H&E) and an increase in adipose tissue (F1:P2 and F2:P3) (Fig. 3A, top row). Internalized nuclei were present in F1:P2. In F1:P1 and F1:P2, numerous nemaline bodies (i.e., rods) were present on Gömöri trichrome (GT; Fig. 3A, second row), which were more prominent in F1:P1 and exclusive to

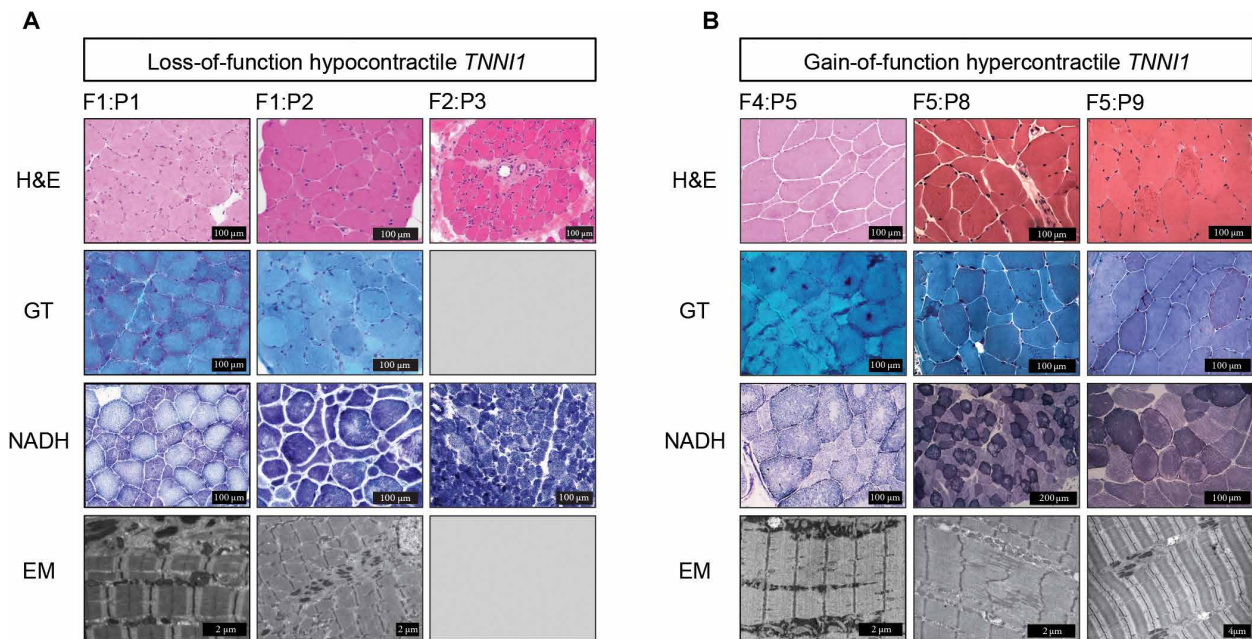


Fig. 3. Histological and electron microscopy findings of patients with *TNNI1* variants. (A) Biopsies from patients F1:P1 (rectus femoris, age 9 years), F1:P2 (rectus femoris, age 10 years), and F2:P3 (vastus lateralis, age 8 months) with loss-of-function hypocontractile *TNNI1* showing H&E (top row), GT (second row), and NADH (third row) stains and electron microscopy (EM) (bottom row). (B) Biopsies from patients F4:P5 (quadriceps, age 35 years), F5:P8 (biceps, age 64 years), and F5:P9 (biceps, age 47 years) with gain-of-function hypercontractile *TNNI1* showing H&E (top row), GT (second row), and NADH (third row) stains and EM (bottom row)

slow-twitch myofibers. Nicotinamide adenine dinucleotide (NADH) staining revealed slow-twitch myofiber hypotrophy in F1:P1 and F2:P3 and core-like regions in F1:P1 and F1:P2 (Fig. 3A, third row). The presence of sarcomeric damage with numerous prominent rods was confirmed on electron microscopy in F1:P1 and F1:P2 (Fig. 3A, bottom row).

Muscle biopsies were also obtained in three patients (F4:P5, F5:P8, and F5:P9) with hypercontractile *TNNI1* disease. All biopsies revealed variation in myofiber size, with an increase in internalized nuclei on H&E (Fig. 3B, top row) and type 1 hypertrophy on NADH (Fig. 3B, third row), consistent with a myopathic disease process. There were eosinophilic granular inclusions on H&E in slow-twitch myofibers (Fig. 3B, top row), which appeared blue-green on GT (Fig. 3B, second row) and appearance of cores, demonstrated by the absence of mitochondria and myosin on NADH (F4:P5, F5:P8, and F5:P9) (Fig. 3B, third row). Electron microscopy confirmed the presence of several rods both in F5:P8 and in F5:P9. There was also ultrastructural evidence of potential core-like regions in the biopsy from F5:P8, with rare streaming of Z-lines (Fig. 3B, bottom row).

Analysis of myofiber size (minFerret) in biopsies from two patients (F1:P1 and F1:P2) with loss-of-function hypocontractile disease and three patients with gain-of-function hypercontractile disease (F4:P5, F5:P8, and F5:P9) did not show a difference between the slow- and fast-twitch myofiber size (fig. S1). Basic demographic information of the control participants used in the morphology analysis is shown in table S3, and minFerret values are in table S4. Thus, histological and ultrastructural findings of a rod myopathy were present in biopsies from both dominant and recessive *TNNI1* patients and were predominantly found in slow-twitch myofibers.

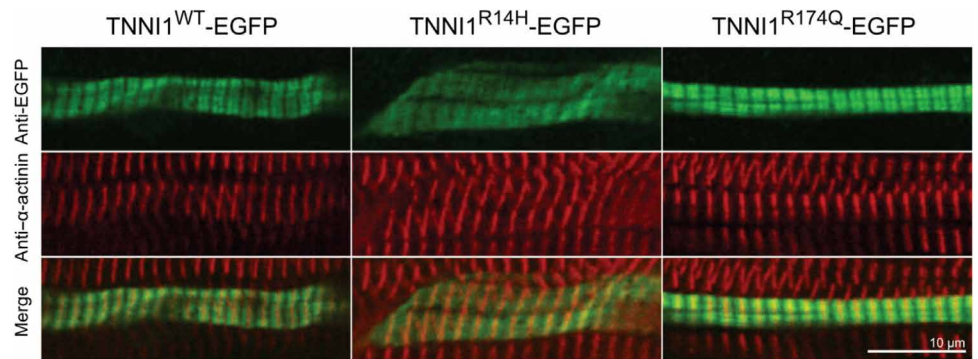
Splicing analysis of *TNNI1* c.190-9G>A

To evaluate the effect of the paternal c.190-9G>A recessive variant on splicing, we performed RNA sequencing on F1:P1 muscle RNA. This revealed a 7-bp extension at the 5' end of exon 6 in a minority of the reads (163 of 3431, 4.7%) (fig. S2A). The splicing anomaly was absent from the control biopsies as well as from 803 muscle samples from GTEx v3. That only a fraction of the reads included the abnormal 7-bp insertion suggested that the c.190-9G>A variant led to nonsense-mediated decay of the paternal allele due to generation of a premature stop codon. Similar allelic skewing toward the maternal allele was also observed at the exon 4 site, because the maternal c.41G>A; p.R14H variant was present in 96% (5416 of 5671) of reads compared with 4% of normal reads at this locus (fig. S2B). Reverse transcription polymerase chain reaction confirmed that the 7-bp insertion was present only on the paternal allele (fig. S2, C and D). Together, these results suggested that the majority of ssTnI molecules in F1:P1's muscles included the p.R14H variant, whereas the paternal allele was severely underrepresented likely because of nonsense-mediated decay after missplicing.

Incorporation of mutant *TNNI1* in zebrafish

To evaluate whether the loss-of-function (R14H) or gain-of-function (R174G) mutant *TNNI1* proteins are effectively incorporated in the thin filaments, we used zebrafish as a well-established model to express sarcomere proteins and to study their in vivo localization. Zebrafish at the one-cell stage were injected with plasmids driving expression of human *TNNI1*, *TNNI1*^{R14H}, or *TNNI1*^{R174Q} tagged with enhanced green fluorescent protein (eGFP) under the control of the muscle-specific unc503 promoter, and after 2 days, we imaged the localization of the mutant proteins. As shown in Fig. 4, zebrafish injected with wild-type (WT)-ssTnI protein showed staining

Fig. 4. Zebrafish muscle expressing wild-type and variant TNNI1-eGFP. Projection through a confocal image series after antibody labeling for eGFP (green) and the z-disk marker α -actinin (red), imaged 2 days after injection. Left shows the localization of WT-ssTnI, the middle shows R14H-ssTnI, and the right shows R174Q-ssTnI.



compatible with thin filament decoration. We noted that the Z-disc staining localized to the middle of the ssTnI staining and the presence of a thin filament bare zone (H-zone) where no staining is present (Fig. 4, left column). Thus, the expressed ssTnI protein was incorporated into the sarcomeres at the anticipated locations. Zebrafish injected with the TNNI1^{R14H} variant also showed the typical striation pattern flanking the Z-discs and the presence of the H-zone (Fig. 4, middle column). However, staining was more diffuse than the sarcomeres expressing TNNI1^{WT}, suggesting that incorporation was slightly decreased, compatible with its loss-of-function mechanism. Zebrafish injected with gain-of-function TNNI1^{R174Q} showed staining of the thin filament that was comparable to that in TNNI1^{WT} fish (Fig. 4, right column), compatible with the gain-of-function mechanistic manifestation.

Molecular dynamics simulations

To study the effects of the variants in *TNNI1* on the structure and dynamics of ssTnI proteins, we performed molecular dynamics (MD) simulations. Because atomistic-resolution structures are not available for human ssTnI, we used the chicken troponin complex (1YTZ) (10) and a chimera, for which residues E4 to R13 were replaced with the human sequence (VERKPKITAS) using CHARMM-GUI (fig. S3A). The R14 position, identified in the patients with recessive hypocontractile disease, was strictly conserved in the ssTnI amino acid sequence. Because functional myofiber analysis could only be performed in family 1, we opted to simulate structures with and without the R14H variant. The dominantly acting R174Q (family 4) and K176del (family 5) variants with hypercontractile disease were found in the C terminus of ssTnI, for which structural data are not yet available (fig. S3A). Therefore, the effect of these variants on structure could not be simulated.

Representative structures for the WT and chimeric troponin complex that are aligned to TnC are shown in Fig. 5A (alignment to TnI is shown in fig. S3B). The global structures expectedly bear high structural similarity as evidenced by the overlap of each protein's backbone structure (Fig. 5A). R14 in both structures localized to D135 in the C terminus of TnC as indicated by the R14/D135 distances of 4.7 ± 0.02 and 4.8 ± 0.03 Å for the chimeric and chicken structures, respectively (Fig. 5B). This interaction reflects favorable electrostatic interactions between the negatively charged TnC D135 residue and the positively charged R14 in the WT structures. This site was conserved in the human cardiac and fast skeletal TnC (fig. S3C).

We did not observe substantial changes in the global structure of the troponin complexes for the R14H variants. However, we did note a decoupling of the histidine substitution at site 14 in TnI from

TnC D135, as shown by the markedly longer (at least 6 Å) distance to D135 relative to WT (Fig. 5, A and B). The decoupling of the site 14 position from D135 appeared to displace the N-terminal TnI α helix from its position in the WT structure relative to the TnC C terminus (fig. S3D).

Previous observations (11–13) indicated that introducing negative charge density, via adding phosphate or aspartic acid, into the N-terminal cTnI/C-terminal cTnC interface reduced the Ca^{2+} sensitivity of force production of sarcomeres. In a similar vein, The R14H variant constitutes a reduction in positive charge within the analogous interface comprising N-terminal ssTnI/C-terminal ssTnC. Therefore, the R14H variant may reduce the Ca^{2+} sensitivity of force generation, which was observed in the results below.

We anticipated that decoupling of N-terminal TnI from C-terminal TnC would affect the structure and dynamics of the TnC N terminus (14). To assess this effect, we used principal components (PC) analysis to identify global motions that manifested in the TnC N terminus; the displacements corresponding to the largest PC are shown in Fig. 5C. The WT, chimera, and chicken isoforms all exhibited similar motions as indicated by their overlapping distributions in the PC1 and PC2 projections (Fig. 5C, right). However, the distribution reported for the chimeric R14H variant was considerably displaced along PC2, which suggested that its N-domain adopted a global position that differed from the WT chimera. We also assessed the root mean square fluctuations within TnC but did not find significant differences (fig. S3E). Thus, the results of the MD simulations warranted additional inquiry to determine whether the changes in structure imposed by the R14H variant interfere with the sarcomere's ability to generate force.

The p.R174Q and the p.K176del variants are in ssTnI's C-terminal extension. This region extends beyond the switch peptide (residues H132 and beyond) and is intrinsically disordered (15) because of its high percentages of positively and negatively charged residues (16). Intrinsically, disordered regions can adopt loose folds, which correlate with the fraction of charged residues within the sequence. Holehouse *et al.* (16) proposed a schematic (see fig. S3F) resembling a phase diagram to categorize these folds as a function of the fractions of negatively charged (y axis) and positively charged amino acids (x axis). Sun and Kekenus-Huskey (17) categorized the intrinsically disordered regions of cTnI (TNNI3), and according to this schematic, the C-terminal domain rests on the border between R2 (coils/premolten globules) and R3 (hairpins/coils/chimera). In fig. S3F, we adapted the Sun and Kekenus-Huskey schematic and demonstrate that the TNNI1 C terminus is similarly positioned along this border (fraction negative and positive are 0.223 and 0.171, respectively).

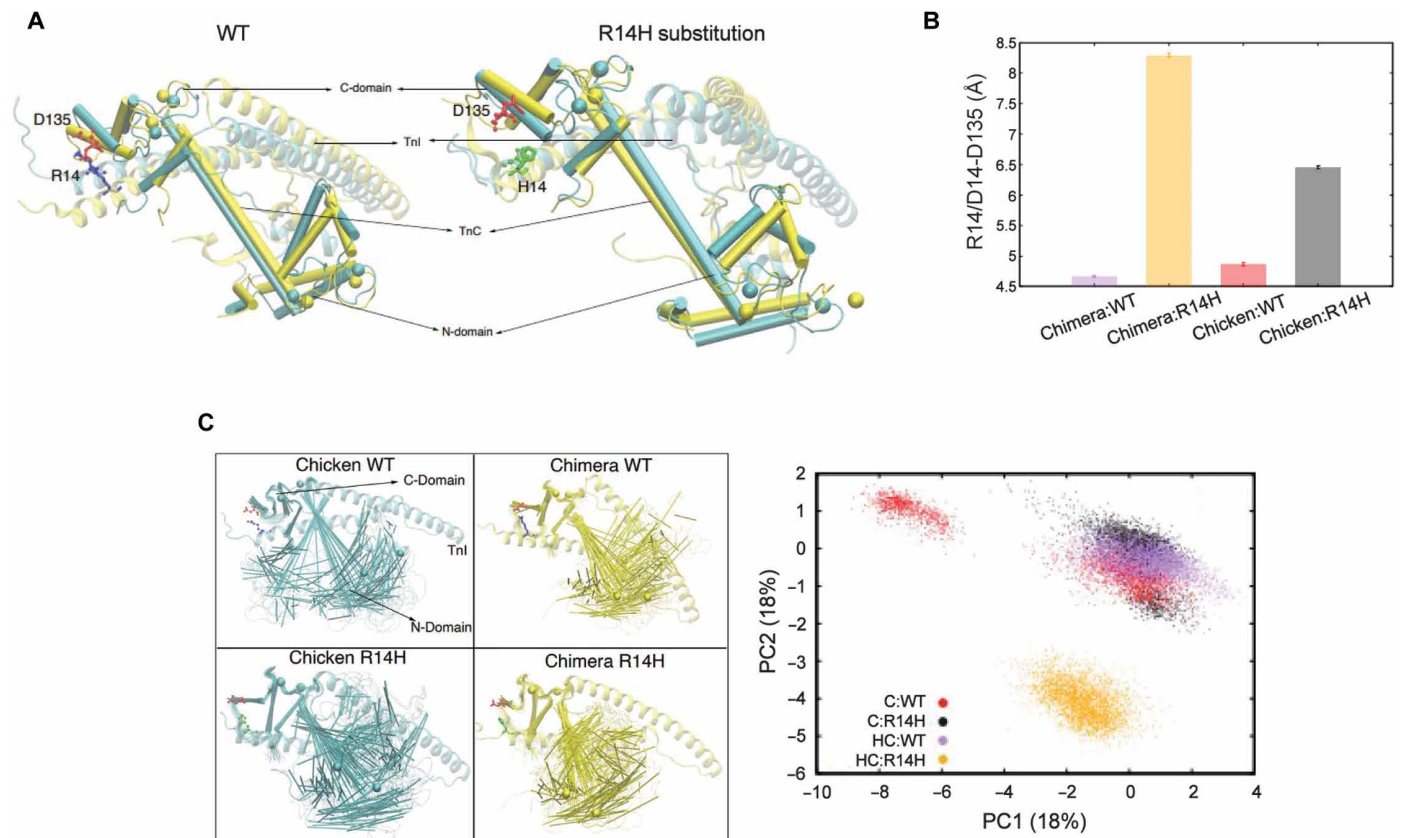


Fig. 5. Molecular dynamics simulations. (A) Comparison of the WT and R14H substitution. WT chicken and chimera are compared by aligning across the TnC's backbone (left). R14H chicken and chimera are compared by aligning across the TnC's backbone (right). Chicken and chimera complexes are represented in cyan and yellow, respectively. TnC and TnI are represented as cartoons and ribbons, respectively. Residues R14 (blue)/H14 (green) and D135 (red) of chicken and human/chicken chimera are represented as ball/stick and licorice, respectively. Calcium ions are shown as spheres. (B) Distance between R14 (TnI) and D135 (TnC). Mean of three MD trials and SEM are shown. Distance is significantly different ($P < 0.001$) between WT and R14H, for both chicken and chimera complexes. (C) Left: All structures were aligned on their respective TnC C-domain and TnI helices. Chicken and chimera complexes are shown in cyan and yellow, respectively. TnC and TnI are represented as cartoons and ribbons, respectively. Residues R14 (blue)/H14 (green) and D135 (red) of chicken and human/chicken chimera are represented as ball/stick and licorice, respectively. Calcium ions are shown as spheres. Right: Projection of principal components 1 and 2 for all structures.

The p.K174Q and p.K176del variants reduce the fractional positively charged amino acid content, which shifts the peptides' ensemble toward the R2 premolten globule state.

Myofiber contractility

To study the effect of the variants on the contractility of sarcomeres, we isolated single myofibers from the patients' muscle biopsies. Biopsy tissue was available from one patient with hypocontractile recessive disease (F1:P1) and one patient with hypercontractile dominant disease (F4:P5). The myofibers were permeabilized, which allows for activation with exogenous Ca^{2+} . Representative myofibers, used for the contractility assays, are shown in Fig. 6, A and B. The myofibers were exposed to incremental $[\text{Ca}^{2+}]$ solutions (Fig. 6C), and the force generated was recorded (Fig. 6D). Results were compared with those from myofibers isolated from biopsies of healthy controls. Data (mean \pm SEM) of slow-twitch myofibers of control participants, F1:P1 and F4:P5, are reported in Table 1, and data (mean \pm SEM) of fast-twitch myofibers are reported in Table 2.

Absolute maximal force (force at pCa 4.5) was significantly lower in slow-twitch myofibers of the patient with recessive disease, F1:P1, compared with those of controls ($P < 0.05$; Table 2). Absolute

maximal force in fast-twitch myofibers was comparable between F1:P1 and controls (Table 2). To account for the differences in myofiber cross-sectional area (CSA), absolute maximal force was normalized to the CSA of the myofiber to obtain specific force. Specific force was significantly lower in slow-twitch myofibers of the patient with hypocontractile recessive disease (F1:P1) compared with those of control participants ($P < 0.05$; Fig. 6E). Specific force in fast-twitch myofibers was comparable between F1:P1 and the control participants (Fig. 6E).

In contrast, in patient F4:P5 with hypercontractile dominant disease, absolute maximal force was increased compared with control levels in slow-twitch myofibers ($P < 0.05$; Table 2). When normalizing absolute maximal force to the CSA, the resulting specific force in F4:P5 slow-twitch myofibers was similar to control levels (Fig. 6E). Furthermore, specific force of fast-twitch myofibers of F4:P5 was comparable to control values (Fig. 6E). In Fig. 6F, the average force- $[\text{Ca}^{2+}]$ relations are shown of slow- and fast-twitch myofibers of F1:P1 (recessive), F4:P5 (dominant), and of control participants. Both F1:P1 slow- and fast-twitch myofibers show a rightward shift of the force- $[\text{Ca}^{2+}]$ relation, indicating a decreased Ca^{2+} sensitivity of force (Fig. 6F) consistent with the manifestation of hypocontractile

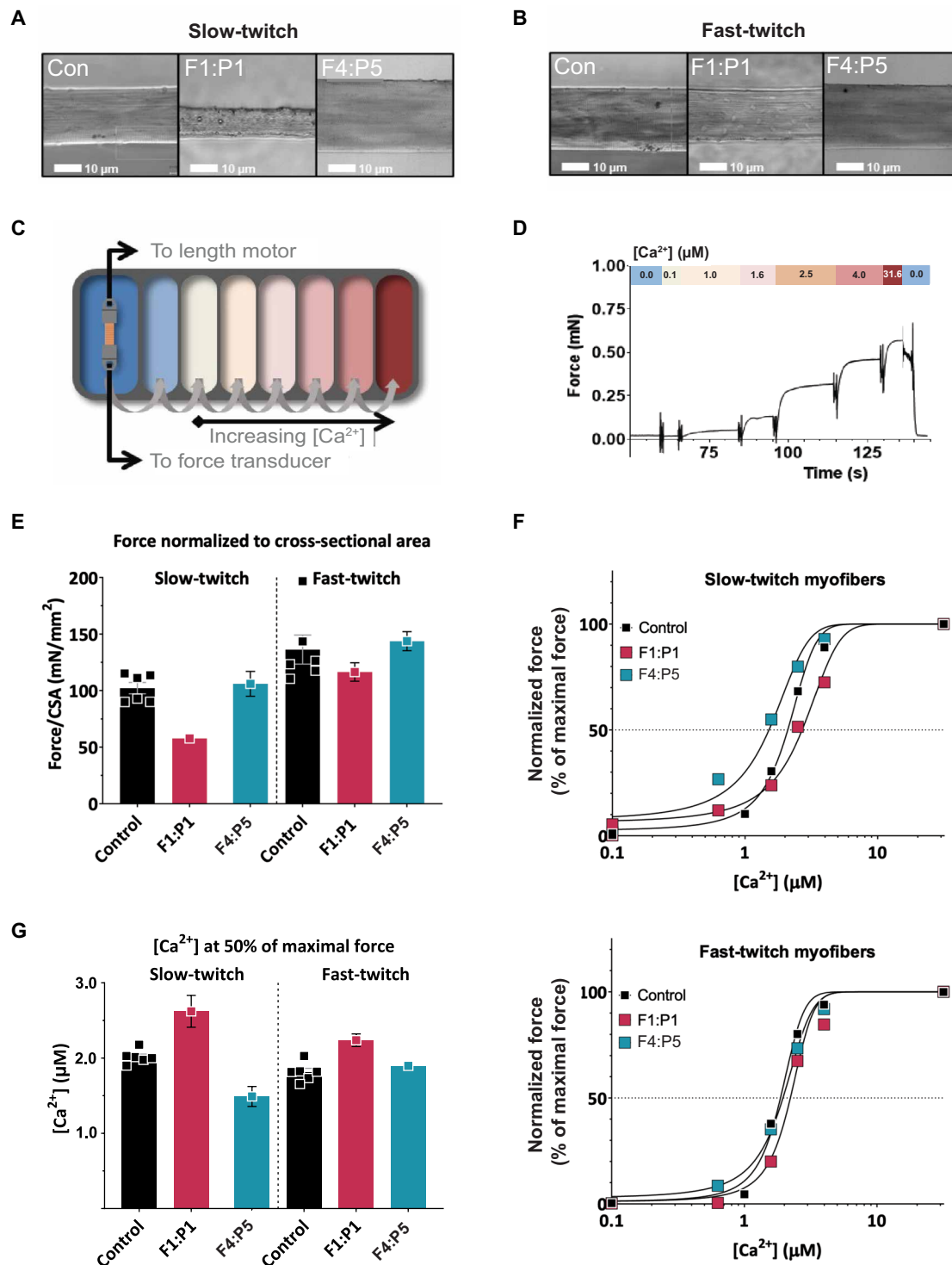


Fig. 6. Myofiber contractility studies. (A) Light microscopy image of a typical example of slow-twitch permeabilized single myofibers isolated from control (Con) and patient (P) biopsy while mounted in the contractility setup. Scale bars, 10 μm . (B) Light microscopy image of a typical example of fast-twitch permeabilized single myofibers isolated from control (Con) and patient (P) biopsy while mounted in the contractility setup. Scale bars, 10 μm . (C) Schematic representation of the contractility setup. An isolated single myofiber clipped in aluminum T-clips is mounted between a force transducer and length motor. The fiber is subsequently moved through the baths filled with solutions with an incremental $[Ca^{2+}]$. (D) Typical tracing showing the force response to the incremental $[Ca^{2+}]$ concentrations. Data shown are from a control myofiber (fast-twitch, CSA = 0.0054 mm²). (E) Maximal active specific force (maximal force normalized to CSA) for myofibers from control, F1:P1, and F4:P5. (F) The force-pCa relation, showing the average curve of slow-twitch (top) and fast-twitch (bottom) control myofibers versus slow-twitch and fast-twitch myofibers from the control, F1:P1, and F4:P5. (G) The $[Ca^{2+}]$ at which 50% of maximum force is reached for control, F1:P1, and F4:P5.

Table 1. Characteristics for control, F1:P1, and F4:P5 slow-twitch myofibers. All data are depicted as mean \pm SEM. The number of measured biopsies (*N*) and single myofibers (*n*) is shown, as well as the percentage change (%) of patient compared with control and the associated *P* value. F, absolute force; $[Ca^{2+}]_{50}$, calcium sensitivity; NS, not significant.

Tissue		C	(N/n)	F1:P1	(N/n)	%P value		F4:P5	(N/n)	%P value	
Absolute maximal force	mN	0.399 \pm 0.073	(6/39)	0.054 \pm 0.013	(1/8)	-86%	0.020	0.729 \pm 0.126	(1/10)	+83%	0.047
Cross-sectional area	mm ²	0.004 \pm 0.001	(6/39)	0.001 \pm 0	(1/8)	-75%	0.002	0.008 \pm 0.002	(1/10)	+100%	NS
Maximal force normalized to CSA	mN/mm ²	102 \pm 5	(6/39)	58 \pm 3	(1/8)	-43%	0.019	106 \pm 11	(1/10)	+4%	NS
$[Ca^{2+}]_{50}$	μ M	2.0 \pm 0.04	(6/37)	2.62 \pm 0.21	(1/8)	+31%	0.001	1.41 \pm 0.14	(1/10)	-30%	0.000

Table 2. Characteristics for control, F1:P1, and F4:P5 fast-twitch myofibers. All data are depicted as mean \pm SEM. The number of measured biopsies (*N*) and single myofibers (*n*) is shown, as well as the percentage change (%) of patient compared with control and the associated *P* value.

Tissue		C	(N/n)	F1:P1	(N/n)	%P value		F4:P5	(N/n)	%P value	
Absolute maximal force	mN	0.591 \pm 0.123	(6/31)	0.592 \pm 0.031	(1/13)	0%	NS	0.57 \pm 0.037	(1/22)	-4%	NS
Cross-sectional area	mm ²	0.004 \pm 0	(6/31)	0.005 \pm 0	(1/13)	+25%	NS	0.004 \pm 0	(1/22)	0%	NS
Maximal force normalized to CSA	mN/mm ²	136 \pm 13	(6/31)	116 \pm 8	(1/13)	-15%	NS	143 \pm 8	(1/22)	+5%	NS
$[Ca^{2+}]_{50}$	μ M	1.81 \pm 0.05	(6/39)	2.24 \pm 0.08	(1/13)	+24%	0.013	1.32 \pm 1.03	(1/22)	-27%	NS

disease. The rightward shift of the force-calcium relation was illustrated by the higher $[Ca^{2+}]_{50}$, the $[Ca^{2+}]$ at which 50% of maximal force is produced. In slow-twitch myofibers of F1:P1, the $[Ca^{2+}]_{50}$ was higher than in the controls ($\Delta = 0.620 \mu\text{M}$, $P < 0.005$; Fig. 6G). In fast-twitch myofibers of F1:P1, the $[Ca^{2+}]_{50}$ was also higher than in controls ($\Delta = 0.43 \mu\text{M}$, $P < 0.05$; Fig. 6G). In contrast, F4:P5 slow-twitch myofiber shows a leftward shift of the force- $[Ca^{2+}]$ relation and a decreased $[Ca^{2+}]_{50}$ compared with control ($\Delta = -0.59 \mu\text{M}$, $P < 0.001$; Fig. 6, F and G), consistent with the manifestation of hypercontractile disease. In F4:P5 fast-twitch fibers, no significant change in $[Ca^{2+}]_{50}$ was observed (Fig. 6G). Thus, the myofiber contractility studies suggested that the patient with the hypocontractile phenotype had reduced maximum force in combination with a reduced sarcomeric force response to submaximal $[Ca^{2+}]$, whereas the patient with the hypercontractile phenotype showed an increased sarcomeric force response to submaximal $[Ca^{2+}]$.

Administration of a slow skeletal muscle troponin activator in loss-of-function hypocontractile *TNNI1*-related disease

Skeletal muscle troponin activators prolong the binding of Ca^{2+} to troponin C on the actin filament of skeletal muscle sarcomeres,

thereby increasing the time during which myosin heads can “find” and bind to binding sites on actin (18). Fast skeletal troponin activators confer specificity for fast-twitch myofibers (18) and thus are of limited value to patients with variants in *TNNI1*, because the contractility of slow-twitch myofibers is predominantly affected. The development of slow skeletal muscle troponin activators, with the goal of exclusively targeting slow-twitch myofibers, is inherently challenging, because several key contractile proteins in slow-twitch myofibers share high sequence similarity with those in cardiac myocytes and may cause undesired cardiac activity. CK-3825076 (fig. S4) is a troponin activator that targets slow-twitch myofibers without affecting the contractility of cardiac myocytes. This selectivity for the targeted myofiber type was confirmed by contractility assays in human myofibers (Fig. 7A and fig. S5, A and B) and by myosin ATPase activity assays (fig. S5A). CK-3825076 was also evaluated in rat cardiomyocytes, and in line with the ATP activity assay (fig. S5A), contractility was unchanged (% change in fractional shortening from baseline: $2.0 \pm 4.1\%$ at $40 \mu\text{M}$).

In human slow-twitch myofibers, CK-3825076 generated close to a maximum force response at a concentration of $\sim 10 \mu\text{M}$ (Fig. 7A), which was then used in the following experiments (note that because

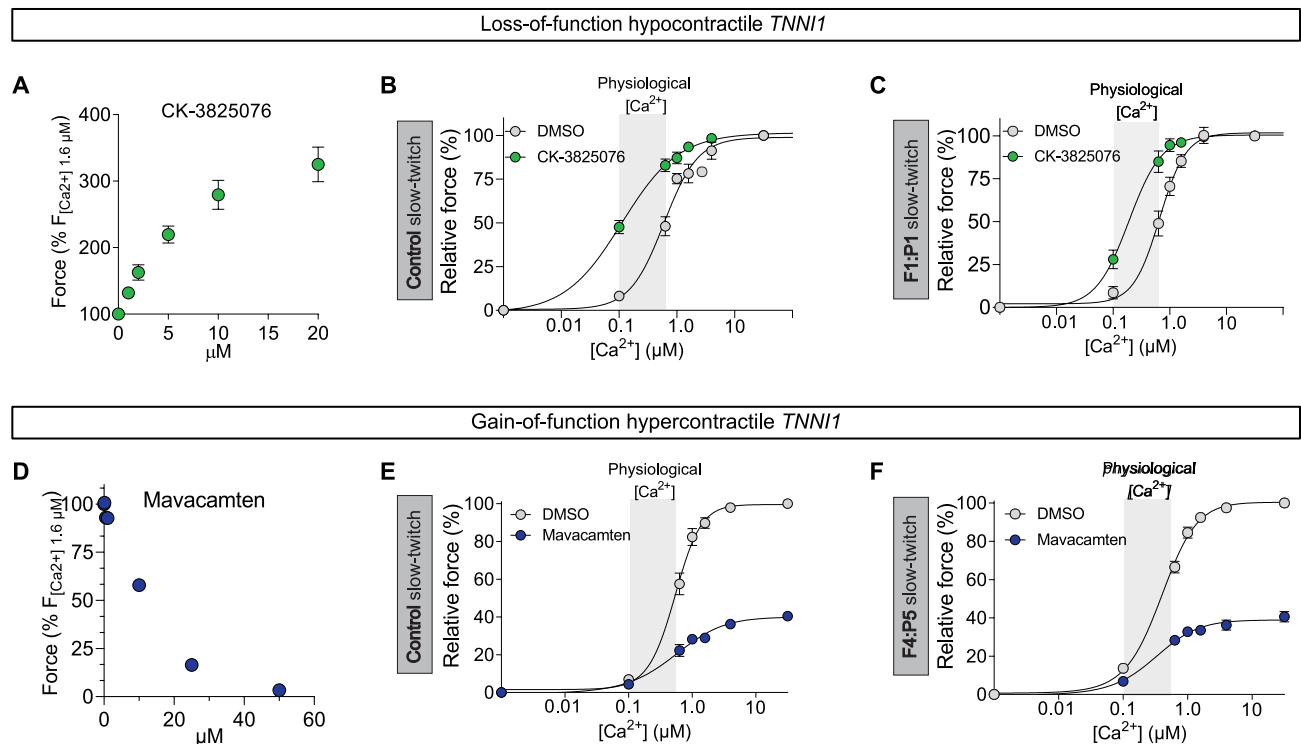


Fig. 7. Administration of a slow skeletal muscle troponin activator and mavacamten to slow-twitch fibers. (A) Slow-twitch human myofibers were exposed to experimental solutions ($[Ca^{2+}] = 1.6 \mu M$) with incremental concentrations of CK-3825076. Force is presented as a percentage of the force generated at a $[Ca^{2+}]$ of $1.6 \mu M$ in the absence of troponin activator [vehicle only, 1% dimethylsulfoxide (DMSO)]. Data are represented as mean and SEM. (B) The effect of $10 \mu M$ CK-3825076 (in 1% DMSO) and DMSO alone on the F-pCa relation in slow-twitch myofibers from a control. The gray bar indicates the range of physiological $[Ca^{2+}]$. (C) The effect of $10 \mu M$ CK-3825076 (in 1% DMSO) and DMSO alone on the F-pCa relation in slow-twitch myofibers from F1:P1. The gray bar indicates the range of physiological $[Ca^{2+}]$. (D) Slow-twitch human myofibers were exposed to experimental solutions ($[Ca^{2+}] = 1.6 \mu M$) with incremental concentrations of mavacamten. Force is presented as a percentage of the force generated at a $[Ca^{2+}]$ of $1.6 \mu M$ in the absence of mavacamten (vehicle only, 1% DMSO). Data are represented as mean and SEM. (E) The effect of $10 \mu M$ mavacamten (in 1% DMSO) and DMSO alone on the F-pCa relation in slow-twitch myofibers from a control. The gray bar indicates the range of physiological $[Ca^{2+}]$. (F) The effect of $10 \mu M$ mavacamten (in 1% DMSO) and DMSO alone on the F-pCa relation in slow-twitch myofibers from F4:P5. The gray bar indicates the range of physiological $[Ca^{2+}]$.

of the limited biopsy size of F1:P2, these experiments were conducted only in myofibers of F1:P1. As shown in (Fig. 7 B and C), CK-3825076 evoked a leftward shift of the force- $[Ca^{2+}]$ relation in slow twitch of both control participants and of patient F1:P1, with no effect on fast-twitch myofibers (fig. S5, B and C). The $[Ca^{2+}]^{50}$ of slow-twitch myofibers was decreased by $0.88 \pm 0.06 \mu M$ in the control and by $0.75 \pm 0.07 \mu M$ in the F1:P1. As expected, maximum force (at $[Ca^{2+}] = 32 \mu M$) was not affected by the troponin activator (Fig. 7, B and C). Thus, the slow skeletal muscle troponin activator augmented force generation at submaximal activation in slow-twitch myofibers in F1:P1 with hypocontractile recessive *TNNI1*-related disease.

Administration of mavacamten in gain-of-function hypercontractile *TNNI1*-related disease

To explore therapeutic interventions aimed at reducing contractility in patients with hypercontractile gain-of-function *TNNI1*-related disease, we studied the effect of mavacamten. Mavacamten, formerly known as MYK-461, is a small-molecule allosteric inhibitor of sarcomeric myosins developed for the treatment of human hypertrophic cardiomyopathy (19–22) that reduces maximal actin-activated myosin ATPase in human β -cardiac myosin (23, 24). β -Cardiac myosin is the dominant myosin isoform in slow-twitch myofibers, rendering mavacamten an attractive small-molecule drug to reduce the hypercontractility in

patients' myofibers with dominant *TNNI1*-related disease. To date, the effect of mavacamten in human slow-twitch myofibers has not been tested. At $10 \mu M$, mavacamten reduced force at submaximal activation in human slow-twitch myofibers (Fig. 7D), a concentration that was then used in the experiments [note that because of the limited biopsy sizes, these experiments were conducted only in myofibers of F4:P5 (p.R174Q) and healthy controls]. In quadriceps, slow-twitch myofibers of a healthy control, mavacamten reduced the force generating capacity by ~60% at all activation levels, including at maximum activation, with no significant effect on the pCa_{50} ($\Delta [Ca^{2+}] = 0.005 \pm 0.02 \mu M$) (Fig. 7E). The force-generating capacity of the hypercontractile slow-twitch myofibers of patient F4:P5 (p.R174Q) was also reduced by ~60% across all activation levels, again with no significant effect on the pCa_{50} ($\Delta [Ca^{2+}] = 0.03 \pm 0.04 \mu M$) (Fig. 7F). A similar effect on contractility was seen in fast-twitch myofibers, expressing *MYH2* isoforms (fig. S5, D and E). Thus, mavacamten reduced force generation in slow-twitch myofibers in F4:P5 (p.R174Q) with hypercontractile dominant *TNNI1*-related disease.

DISCUSSION

In this study, we established *TNNI1* as a gene associated with early-onset muscle disease in humans. We identified and characterized both

recessive loss-of-function and dominant gain-of-function pathogenic variants in *TNNI1*. Aligned with the recessive and dominant genetic mechanisms of the *TNNI1* variants, we discovered a corresponding dichotomy of pathophysiological mechanisms consisting of altered Ca^{2+} sensitivity of force that result in distinct hypo- and hypercontractile phenotypes that are reflected in the clinical disease and therapeutic approach (fig. S6). Variant-specific disease mechanisms underlying altered muscle contractility are emerging for specific pathogenic sarcomeric gene variants (25–28). In this study, we found both mechanisms to be relevant for *TNNI1*.

The equivalent of the gain-of-function p.K176del *TNNI1* variant (family 5) has also been identified in *TNNI2*, encoding the fast-twitch troponin I isoform, in a family with arthrogryposis and mild myopathy (29), although its functional consequence was not investigated. The equivalent p.R174Q gain-of-function *TNNI1* variant identified in family 4 was also previously identified in heterozygosity in *TNNI2*, in two families with dominantly inherited multiple congenital contracture syndrome (30). In line with our contractility studies, the p.R174Q *TNNI2* variant also increased the Ca^{2+} sensitivity of force. Moreover, consistent with the fiber-type-specific expression of *TNNI1* and *TNNI2*, altered Ca^{2+} sensitivity was restricted to the associated fiber type (31). Our data would also support the hypothesis postulated by Nishimori *et al.* (3), who suspected that an increased Ca^{2+} sensitivity of force was the underlying disease mechanism of a presumed gain-of-function c.523A>T, p.K175* *TNNI1* variant in a family with arthrogryposis and elevated CK.

We hypothesize that the gain-of-function *TNNI1* variants result in continuous hypercontractility of the muscle fibers, ultimately leading to eccentric damage and subsequent sarcomeric myofiber degeneration as seen histologically and ultrastructurally and reflected by CK elevations. Over time, the regeneration mechanism exhausts itself, resulting in muscle weakness, as was noted in family 5 (p.K176del). This is in contrast with the primary weakness and myopathic but nondystrophic process that is associated with the hypocontractile phenotype seen in patients with recessive *TNNI1* loss-of-function variants. Consistent with the expression of *TNNI1* in slow-twitch fibers, the rod pathology was predominantly found in type 1 slow-twitch fibers, in both hypo- (F1 and F2) and hypercontractile (F5) biopsies.

In line with a direct pathogenic effect of the *TNNI1* variants on TnI, we found that in zebrafish, both the recessive hypocontractile (p.R14H) and dominant hypercontractile (p.R174Q) variants incorporated into the sarcomeric thin filaments. This supports a direct pathogenic effect, specifically of the hypercontractile p.R174Q variant on the contractility of myofibers rather than indirect effects secondary to a TnI deficiency. The MD simulations indicate that the underlying molecular pathomechanism of the p.R14H variant includes a decoupling of TnI from TnC that displaces the N-terminal TnI α helix relative to the TnC C terminus. In line with previous work (32–34), the p.R14H variant constitutes a reduction in positive charge within the analogous interface comprising N-terminal ssTnI/C-terminal ssTnC and may therefore underlie the observed reduction in the Ca^{2+} sensitivity of force. For the gain-of-function p.K174Q variant, we postulate that the conformational shift away from the boundary favors the association of the switch peptide with TnC relative to the WT (fig. S3F). This interpretation is consistent with the reduction in the fractional positive charge affected by the cTnI variants p.K178E and p.R192H, resulting in substantial increases in calcium sensitivity in skinned fiber preparations (35). The previously

reported p.K175* *TNNI1* variant resulting in a hypercontractile phenotype was shown to escape nonsense-mediated decay, with a truncated transcript identified in patient muscle (3). This variant is flanked by the gain-of-function variants reported here (p.R174Q and p.K176del), suggesting that its pathomechanism is also associated with a reduction in the fractional positively charged amino acid content.

The recessive recurrent p.R14C substitution was present in two families and manifests with profound and progressive muscle weakness (F2:P3). The same residue was found to be altered in family 1 (p.R14H/c.190-9G>A). Although symptom onset and progression were milder as compared with F2 and F3, patients still showed evidence of progression. We hypothesize that there may be some residual “leaky” normal splicing from the c.190-9G>A allele, ameliorating disease severity in this family. This would suggest that even a low level of normal troponin I expression may result in significant clinical benefit.

We show that administration of a slow skeletal muscle troponin activator increased force generation at submaximal activation levels in slow-twitch myofibers of F1:P1. Activators of slow-twitch myofibers, such as CK-3825076, have the potential to be of considerable clinical benefit, because this myofiber type is recruited first during normal muscle activation (36). The development of these activators has been challenging, because several key contractile proteins in slow-twitch myofibers and cardiomyocytes have a high sequence similarity. Even at high concentrations, CK-3825076 does not affect cardiac contractility, illustrating the promise of this compound not only for recessive loss-of-function *TNNI1*-related disease but also for other genetic and acquired diseases that affect slow-twitch myofibers (37). Future studies should address whether therapeutic concentrations of slow skeletal muscle troponin activators are well tolerated and safe. For patients with dominant hypercontractile gain-of-function *TNNI1* variants, we showed that mavacamten is able to reduce the contractility of slow-twitch myofibers by ~60% across all activation levels (Fig. 7), thereby restoring the increased absolute myofiber force of F4:P5 (R174Q) patient myofibers to normal levels (Fig. 4 and Table 1). The current study shows the successful application of mavacamten in human myofibers. Mavacamten is approved for the treatment of hypertrophic cardiomyopathy and inhibits cardiac myosin (MYH7) ATPase (19, 38) to reduce sarcomere hypercontractility (23, 24). Concentrations used in the present study exceed those used in the treatment of patients with hypertrophic cardiomyopathy (19); therefore, the cardiac safety profile of this approach in *TNNI1*-related disease needs careful consideration. We also observed an effect of mavacamten on contractility of human fast-twitch myofibers, expressing *MYH2* isoforms. This effect was of a similar magnitude as that observed in slow-twitch myofibers and suggests that, in humans, mavacamten equally affects slow- and fast-twitch myofibers. Overall, the mavacamten findings provide proof of concept for a rational approach to hypercontractility in patients with *TNNI1*-related disease justifying further investigation.

We note limitations to our study, particularly the still small number of clinical observations so that the full spectrum of *TNNI1*-related disease remains to be established, including potential cardiac implications. Also, our investigation of therapeutic strategies was limited to in vitro studies; an appropriate animal model will need to be generated to explore in vivo implications.

In conclusion, we have provided detailed characterization of patients with pathogenic *TNNI1* variants and have established distinct

pathomechanisms for recessive loss-of-function and dominant gain-of-function variants in *TNNI1*, manifesting as either a hypo- or a hypercontractile sarcomeric disease, respectively. We highlighted the successful application of a slow skeletal muscle troponin activator and mavacamten to normalize physiological force generation in myofiber studies of recessive and dominant *TNNI1* variants, respectively, suggesting future treatment strategies.

MATERIALS AND METHODS

Study design

The purpose of this study was to apply next-generation-based sequencing to clinically and histologically well-characterized patients with rare neuromuscular diseases, who were enrolled in Institutional Review Board (IRB)-approved protocols, to identify the underlying genetic etiology. The effect of the identified *TNNI1* variants was studied in (blinded) zebrafish studies (ERM22161 approved by the Monash Animal Research Platform) and through MD and fiber contractility studies, which included a therapeutic proof-of-concept approach.

Patient recruitment and sample collection

Patients were identified by their neurologist or geneticist. Written informed consent and age-appropriate assent for study procedures were obtained by a qualified investigator [protocol 12-N-0095 approved by the National Institute of Neurological Disorders and Stroke, National Institutes of Health IRB, protocol 2019-199-f-S, and protocol RA/4/20/1008 approved by the University of Western Australia (UWA) Human Research Ethics Committee protocol, Medical Research Ethics Committee of the National Research Center, registration number: 16-100]. Medical history was obtained, and clinical evaluations, including muscle MRI and muscle biopsy, were performed as part of the standard diagnostic examination. Samples for research-based testing, including muscle and blood, were obtained using standard procedures. Family 2, family 3, and family 5 were identified through GeneMatcher (39).

Statistical analysis

Permeabilized myofiber contractility data were tested for significance by performing a mixed model analysis with a random effect for biopsies and post hoc tests with a Bonferroni correction, after checking whether the residues were normally distributed. Testing was performed using the software package SPSS.

Supplementary Materials

This PDF file includes:

Supplementary methods

Figs. S1 to S6

Tables S1 to S4

References (40–67)

Other Supplementary Material for this manuscript includes the following:

Data file S1

MDAR Reproducibility Checklist

REFERENCES AND NOTES

- A. M. Gordon, E. Homsher, M. Regnier, Regulation of contraction in striated muscle. *Physiol. Rev.* **80**, 853–924 (2000).
- M. van de Locht, T. C. Borsboom, J. M. Winter, C. A. C. Ottenheijm, Troponin variants in congenital myopathies: How they affect skeletal muscle mechanics. *Int. J. Mol. Sci.* **22**, 9187 (2021).
- Y. Nishimori, A. Iida, M. Ogasawara, M. Okubo, Y. Yonenobu, M. Kinoshita, K. Sugie, S. Noguchi, I. Nishino, *TNNI1* Mutated in autosomal dominant proximal arthrogyrosis. *Neurol. Genet.* **8**, e649 (2022).
- R. Wade, R. Eddy, T. B. Shows, L. Kedes, cDNA sequence, tissue-specific expression, and chromosomal mapping of the human slow-twitch skeletal muscle isoform of troponin I. *Genomics* **7**, 346–357 (1990).
- S. Sasse, N. J. Brand, P. Kyprianou, G. K. Dhoot, R. Wade, M. Arai, M. Periasamy, M. H. Yacoub, P. J. Barton, Troponin I gene expression during human cardiac development and in end-stage heart failure. *Circ. Res.* **72**, 932–938 (1993).
- J. Ochala, Thin filament proteins mutations associated with skeletal myopathies: Defective regulation of muscle contraction. *J. Mol. Med.* **86**, 1197–1204 (2008).
- N. F. Clarke, Skeletal muscle disease due to mutations in tropomyosin, troponin and cofilin. *Adv. Exp. Med. Biol.* **642**, 40–54 (2008).
- J. Mogensen, T. Hey, S. Lambrecht, A systematic review of phenotypic features associated with cardiac troponin I mutations in hereditary cardiomyopathies. *Can. J. Cardiol.* **31**, 1377–1385 (2015).
- J. D. Wittenbach, B. T. Cocanougher, P. Yun, A. R. Foley, C. G. Bönnemann, Muscleviz: Free open-source software for muscle weakness visualization. *J. Neuromuscul. Dis.* **6**, 263–266 (2019).
- M. V. Vinogradova, D. B. Stone, G. G. Malanina, C. Karatzafiri, R. Cooke, R. A. Mendelson, R. J. Fletterick, Ca^{2+} -regulated structural changes in troponin. *Proc. Natl. Acad. Sci. U.S.A.* **102**, 5038–5043 (2005).
- B. J. Biesiadecki, T. Kobayashi, J. S. Walker, R. J. Solaro, P. P. de Tombe, The troponin C G159D mutation blunts myofilament desensitization induced by troponin I Ser23/24 phosphorylation. *Circ. Res.* **100**, 1486–1493 (2007).
- S. E. Lang, J. Schwank, T. K. Stevenson, M. A. Jensen, M. V. Westfall, Independent modulation of contractile performance by cardiac troponin I Ser43 and Ser45 in the dynamic sarcomere. *J. Mol. Cell. Cardiol.* **79**, 264–274 (2015).
- M. V. Westfall, I. Turner, F. P. Albayya, J. M. Metzger, Troponin I chimera analysis of the cardiac myofilament tension response to protein kinase A. *Am. J. Physiol. Cell Physiol.* **280**, C324–C332 (2001).
- Z. Mahmud, P. S. Dhami, C. Rans, P. B. Liu, P. M. Hwang, Dilated cardiomyopathy mutations and phosphorylation disrupt the active orientation of cardiac troponin C. *J. Mol. Biol.* **433**, 167010 (2021).
- J.-J. Sheng, J.-P. Jin, *TNNI1*, *TNNI2* and *TNNI3*: Evolution, regulation, and protein structure-function relationships. *Gene* **576**, 385–394 (2016).
- A. S. Holehouse, R. K. Das, J. N. Ahad, M. O. Richardson, R. V. Pappu, CIDER: Resources to analyze sequence-ensemble relationships of intrinsically disordered proteins. *Biophys. J.* **112**, 16–21 (2017).
- B. Sun, P. M. Kekenus-Huskey, Myofilament-associated proteins with intrinsic disorder (MAPIDs) and their resolution by computational modeling. *Q. Rev. Biophys.* **56**, e2 (2023).
- A. J. Russell, J. J. Hartman, A. C. Hinken, A. R. Muci, R. Kawas, L. Driscoll, G. Godinez, K. H. Lee, D. Marquez, W. F. Browne IV, M. M. Chen, D. Clarke, S. E. Collibee, M. Garard, R. Hansen, Z. Jia, P.-P. Lu, H. Rodriguez, K. G. Saikali, J. Schaletzky, V. Vijayakumar, D. L. Albertus, D. R. Claffin, D. J. Morgans, B. P. Morgan, F. I. Malik, Activation of fast skeletal muscle troponin as a potential therapeutic approach for treating neuromuscular diseases. *Nat. Med.* **18**, 452–455 (2012).
- I. Olivotto, A. Oreziak, R. Barriales-Villa, T. P. Abraham, A. Masri, P. Garcia-Pavia, S. Saberi, N. K. Lakdawala, M. T. Wheeler, A. Owens, M. Kubanek, W. Wojakowski, M. K. Jensen, J. Gimeno-Blanes, K. Afshar, J. Myers, S. M. Hegde, S. D. Solomon, A. J. Sehnert, D. Zhang, W. Li, M. Bhattacharya, J. M. Edelberg, C. B. Waldman, S. J. Lester, A. Wang, C. Y. Ho, D. Jacoby; EXPLORER-HCM study investigators, Mavacamten for treatment of symptomatic obstructive hypertrophic cardiomyopathy (EXPLORER-HCM): A randomised, double-blind, placebo-controlled, phase 3 trial. *Lancet* **396**, 759–769 (2020).
- E. M. Green, H. Wakimoto, R. L. Anderson, M. J. Evanchik, J. M. Gorham, B. C. Harrison, M. Henze, R. Kawas, J. D. Oslob, H. M. Rodriguez, Y. Song, W. Wan, L. A. Leinwand, J. A. Spudich, R. S. McDowell, J. G. Seidman, C. E. Seidman, A small-molecule inhibitor of sarcomere contractility suppresses hypertrophic cardiomyopathy in mice. *Science* **351**, 617–621 (2016).
- J. A. Spudich, T. Aksel, S. R. Bartholomew, S. Nag, M. Kawana, E. C. Yu, S. S. Sarkar, J. Sung, R. F. Sommese, S. Sutton, C. Cho, A. S. Adhikari, R. Taylor, C. Liu, D. Trivedi, K. M. Ruppel, Effects of hypertrophic and dilated cardiomyopathy mutations on power output by human β -cardiac myosin. *J. Exp. Biol.* **219**, 161–167 (2016).
- K. Alsulami, S. Marston, Small molecules acting on myofilaments as treatments for heart and skeletal muscle diseases. *Int. J. Mol. Sci.* **21**, 9599 (2020).
- R. L. Anderson, D. V. Trivedi, S. S. Sarkar, M. Henze, W. Ma, H. Gong, C. S. Rogers, J. M. Gorham, F. L. Wong, M. M. Morck, J. G. Seidman, K. M. Ruppel, T. C. Irving, R. Cooke, E. M. Green, J. A. Spudich, Deciphering the super relaxed state of human β -cardiac myosin and the mode of action of mavacamten from myosin molecules to muscle fibers. *Proc. Natl. Acad. Sci. U.S.A.* **115**, E8143–E8152 (2018).
- J. A. Rohde, O. Roopnarine, D. D. Thomas, J. M. Muretta, Mavacamten stabilizes an autoinhibited state of two-headed cardiac myosin. *Proc. Natl. Acad. Sci. U.S.A.* **115**, E7486–E7494 (2018).

25. A. E. Davidson, F. M. Siddiqui, M. A. Lopez, P. Lunt, H. A. Carlson, B. E. Moore, S. Love, D. E. Born, H. Roper, A. Majumdar, S. Jayadev, H. R. Underhill, C. O. Smith, M. von der Hagen, A. Hubner, P. Jardine, A. Merrison, E. Curtis, T. Cullup, H. Jungbluth, M. O. Cox, T. L. Winder, H. Abdel Salam, J. Z. Li, S. A. Moore, J. J. Dowling, Novel deletion of lysine 7 expands the clinical, histopathological and genetic spectrum of TPM2-related myopathies. *Brain* **136**, 508–521 (2013).
26. S. Donkervoort, M. Papadakis, J. M. de Winter, M. B. Neu, J. Kirschner, V. Bolduc, M. L. Yang, M. A. Gibbons, Y. Hu, J. Dastgir, M. E. Leach, A. Rutkowski, A. R. Foley, M. Krüger, E. P. Wartchow, E. M. Namara, R. Ong, K. J. Nowak, N. G. Laing, N. F. Clarke, C. Ottenheijm, S. B. Marston, C. G. Bönnemann, TPM3 deletions cause a hypercontractile congenital muscle stiffness phenotype. *Ann. Neurol.* **78**, 982–994 (2015).
27. N. Mokbel, B. Ilkovi, M. Kreissl, M. Memo, C. M. Jeffries, M. Marttila, V. L. Lehtokari, E. Lemola, M. Gronholm, N. Yang, D. Menard, P. Marcorelles, A. Echaniz-Laguna, J. Reimann, M. Vainzof, N. Monnier, G. Ravenscroft, E. McNamara, K. J. Nowak, N. G. Laing, C. Wallgren-Pettersson, J. Trewthella, S. Marston, C. Ottenheijm, K. N. North, N. F. Clarke, K7del is a common TPM2 gene mutation associated with nemaline myopathy and raised myofibre calcium sensitivity. *Brain* **136**, 494–507 (2013).
28. M. van de Locht, S. Donkervoort, J. M. de Winter, S. Conijn, L. Begthel, B. Kusters, P. Mohassel, Y. Hu, L. Medne, C. Quinn, S. A. Moore, A. R. Foley, G. Seo, D. T. Hwee, F. I. Malik, T. Irving, W. Ma, H. L. Granzier, E. J. Kamsteeg, K. Immadisetty, P. Kekenes-Huskey, J. R. Pinto, N. Voermans, C. G. Bönnemann, C. A. Ottenheijm, Pathogenic variants in TNNC2 cause congenital myopathy due to an impaired force response to calcium. *J. Clin. Invest.* **131**, e145700 (2021).
29. E. Kimber, H. Tajsharghi, A. K. Kroksmark, A. Oldfors, M. Tulinius, A mutation in the fast skeletal muscle troponin I gene causes myopathy and distal arthrogryposis. *Neurology* **67**, 597–601 (2006).
30. S. J. Sung, A. M. Brassington, K. Grannatt, A. Rutherford, F. G. Whitby, P. A. Krakowiak, L. B. Jorde, J. C. Carey, M. Bamshad, Mutations in genes encoding fast-twitch contractile proteins cause distal arthrogryposis syndromes. *Am. J. Hum. Genet.* **72**, 681–690 (2003).
31. P. Robinson, S. Lipscomb, L. C. Preston, E. Altin, H. Watkins, C. C. Ashley, C. S. Redwood, Mutations in fast skeletal troponin I, troponin T, and beta-tropomyosin that cause distal arthrogryposis all increase contractile function. *FASEB J.* **21**, 896–905 (2007).
32. S. Jo, T. Kim, V. G. Iyer, W. Im, CHARMM-GUI: A web-based graphical user interface for CHARMM. *J. Comput. Chem.* **29**, 1859–1865 (2008).
33. J. Lee, X. Cheng, J. M. Swails, M. S. Yeom, P. K. Eastman, J. A. Lemkul, S. Wei, J. Buckner, J. C. Jeong, Y. Qi, S. Jo, V. S. Pande, D. A. Case, C. L. Brooks III, A. D. MacKerell Jr., J. B. Klauda, W. Im, CHARMM-GUI input generator for NAMD, GROMACS, AMBER, OpenMM, and CHARMM/OpenMM simulations using the CHARMM36 additive force field. *J. Chem. Theory Comput.* **12**, 405–413 (2016).
34. D. G. Vassilyev, S. Takeda, S. Wakatsuki, K. Maeda, Y. Maéda, Crystal structure of troponin C in complex with troponin I fragment at 2.3-Å resolution. *Proc. Natl. Acad. Sci. U.S.A.* **95**, 4847–4852 (1998).
35. A. V. Gomes, J. Liang, J. D. Potter, Mutations in human cardiac troponin I that are associated with restrictive cardiomyopathy affect basal ATPase activity and the calcium sensitivity of force development. *J. Biol. Chem.* **280**, 30909–30915 (2005).
36. E. Henneman, Relation between size of neurons and their susceptibility to discharge. *Science* **126**, 1345–1347 (1957).
37. H. Jungbluth, S. Treves, F. Zorzato, A. Sarkozy, J. Ochala, C. Sewry, R. Phadke, M. Gautel, F. Muntoni, Congenital myopathies: Disorders of excitation-contraction coupling and muscle contraction. *Nat. Rev. Neurol.* **14**, 151–167 (2018).
38. M. Papadakis, J. Basu, S. Sharma, Mavacamten: Treatment aspirations in hypertrophic cardiomyopathy. *Lancet* **396**, 736–737 (2020).
39. N. Sobreira, F. Schiettecatte, D. Valle, A. Hamosh, GeneMatcher: A matching tool for connecting investigators with an interest in the same gene. *Hum. Mutat.* **36**, 928–930 (2015).
40. K. J. Karczewski, L. C. Francioli, G. Tiao, B. B. Cummings, J. Alfoldi, Q. Wang, R. L. Collins, K. M. Laricchia, A. Ganna, D. P. Birnbaum, L. D. Gauthier, H. Brand, M. Solomonson, N. A. Watts, D. Rhodes, M. Singer-Berk, E. M. England, E. G. Seaby, J. A. Kosmicki, R. K. Walters, K. Tashman, Y. Farjoun, E. Banks, T. Poterba, A. Wang, C. Seed, N. Whiffin, J. X. Chong, K. E. Samocha, E. Pierce-Hoffman, Z. Zappala, A. H. O'Donnell-Luria, E. V. Minikel, B. Weisburd, M. Lek, J. S. Ware, C. Vittal, I. M. Armean, L. Bergelson, K. Cibulskis, K. M. Connolly, M. Covarrubias, S. Donnelly, S. Ferreira, S. Gabriel, J. Gentry, N. Gupta, T. Jeandet, D. Kaplan, C. Llanwarne, R. Munshi, S. Novod, N. Petrillo, D. Roazen, V. Ruano-Rubio, A. Saltzman, M. Schleicher, J. Soto, K. Tibbetts, C. Tolonen, G. Wade, M. E. Talkowski; Genome Aggregation Database Consortium, B. M. Neale, M. J. Daly, D. G. M. Arthur, The mutational constraint spectrum quantified from variation in 141,456 humans. *Nature* **581**, 434–443 (2020).
41. J. H. Park, C. Elpers, J. Reunert, M. L. McCormick, J. Mohr, S. Biskup, O. Schwartz, S. Rust, M. Gruneberg, A. Seelhofer, U. Schara, E. Boltshauser, D. R. Spitz, T. Marquardt, SOD1 deficiency: A novel syndrome distinct from amyotrophic lateral sclerosis. *Brain* **142**, 2230–2237 (2019).
42. S. J. Beecroft, K. S. Yau, R. J. N. Allcock, K. Mina, R. Gooding, F. Faiz, V. J. Atkinson, C. Wise, P. Sivadurai, D. Trajanoski, N. Kresoje, R. Ong, R. M. Duff, M. Cabrera-Serrano, K. J. Nowak, N. Pachter, G. Ravenscroft, P. J. Lamont, M. R. Davis, N. G. Laing, Targeted gene panel use in 2249 neuromuscular patients: The Australasian referral center experience. *Ann. Clin. Transl. Neurol.* **7**, 353–362 (2020).
43. G. Ravenscroft, J. S. Clayton, F. Faiz, P. Sivadurai, D. Milnes, R. Cincotta, P. Moon, B. Kamien, M. Edwards, M. Delatycki, P. J. Lamont, S. H. Chan, A. Colley, A. Ma, F. Collins, L. Henington, T. Zhao, G. McGillivray, S. Ghedia, K. Chao, A. O'Donnell-Luria, N. G. Laing, M. R. Davis, Neurogenetic fetal akinesia and arthrogryposis: Genetics, expanding genotype-phenotypes and functional genomics. *J. Med. Genet.* **58**, 609–618 (2021).
44. J. Schindelin, I. Arganda-Carreras, E. Frise, V. Kaynig, M. Longair, T. Pietzsch, S. Preibisch, C. Rueden, S. Saalfeld, B. Schmid, J. Y. Tinevez, D. J. White, V. Hartenstein, K. Eliceiri, P. Tomancak, A. Cardona, Fiji: An open-source platform for biological-image analysis. *Nat. Methods* **9**, 676–682 (2012).
45. J. Berger, P. D. Currie, 503unc, a small and muscle-specific zebrafish promoter. *Genesis* **51**, 443–447 (2013).
46. A. Matsuda, T. Koujin, L. Schermelleh, T. Haraguchi, Y. Hiraoka, High-accuracy correction of 3D chromatic shifts in the age of super-resolution biological imaging using chromagnon. *J. Vis. Exp.*, 10.3791/60800, (2020).
47. S. Jo, T. Kim, W. Im, Automated builder and database of protein/membrane complexes for molecular dynamics simulations. *PLOS ONE* **2**, e880 (2007).
48. Y. Qi, X. Cheng, W. Han, S. Jo, K. Schulten, W. Im, CHARMM-GUI PACE CG Builder for solution, micelle, and bilayer coarse-grained simulations. *J. Chem. Inf. Model.* **54**, 1003–1009 (2014).
49. W. L. Jorgensen, J. Chandrasekhar, J. D. Madura, R. W. Impey, M. L. Klein, Comparison of simple potential functions for simulating liquid water. *J. Chem. Phys.* **79**, 926–935 (1983).
50. J. B. Klauda, R. M. Venable, J. A. Freites, J. W. O'Connor, D. J. Tobias, C. Mondragon-Ramirez, I. Vorobyov, A. D. MacKerell Jr., R. W. Pastor, Update of the CHARMM all-atom additive force field for lipids: Validation on six lipid types. *J. Phys. Chem. B* **114**, 7830–7843 (2010).
51. D. A. Case, I. Y. Ben-Shalom, S. R. Brozell, D. S. Cerutti, I. T. E. Cheatham, V. W. D. Cruzeiro, T. A. Darden, (University of California, San Francisco, 2018).
52. J. K. Reid, *Large Sparse Sets of Linear Equations: On the Method of Conjugate Gradients for the Solution of Large Sparse System of Linear Equations*. (Academic Press, London, 1971).
53. S. E. Feller, Y. Zhang, R. W. Pastor, B. R. Brooks, Constant pressure molecular dynamics simulation: The Langevin piston method. *J. Chem. Phys.* **103**, 4613–4621 (1995).
54. G. J. Martyna, D. J. Tobias, M. L. Klein, Constant pressure molecular dynamics algorithms. *J. Chem. Phys.* **101**, 4177–4189 (1994).
55. J.-P. Ryckaert, G. Cicciotti, H. J. C. Berendsen, Numerical integration of the cartesian equations of motion of a system with constraints: Molecular dynamics of n-alkanes. *J. Comput. Phys.* **23**, 327–341 (1977).
56. T. Darden, D. York, L. Pedersen, Particle mesh Ewald: AnN-log(N) method for Ewald sums in large systems. *J. Chem. Phys.* **98**, 10089–10092 (1993).
57. W. Humphrey, A. Dalke, K. Schulten, VMD: Visual molecular dynamics. *J. Mol. Graph.* **14**, 27–38 (1996).
58. M. Yahyavi, S. Falsafi-Zadeh, Z. Karimi, G. Kalatari, H. Galehdari, VMD-SS: A graphical user interface plug-in to calculate the protein secondary structure in VMD program. *Bioinformatics* **10**, 548–550 (2014).
59. S. J. Beecroft, M. van de Locht, J. M. de Winter, C. A. Ottenheijm, C. A. Sewry, S. Mohammed, M. M. Ryan, I. R. Woodcock, L. Sanders, R. Gooding, M. R. Davis, E. C. Oates, N. G. Laing, G. Ravenscroft, C. A. McLean, H. Jungbluth, Recessive MYH7-related myopathy in two families. *Neuromuscul. Disord.* **29**, 456–467 (2019).
60. C. A. Ottenheijm, D. Buck, J. M. de Winter, C. Ferrara, N. Pirodoli, C. Tesi, J. R. Jasper, F. I. Malik, H. Meng, G. J. Stienen, A. H. Beggs, S. Labeit, C. Poggesi, M. W. Lawlor, H. Granzier, Deleting exon 55 from the nebulin gene induces severe muscle weakness in a mouse model for nemaline myopathy. *Brain* **136**, 1718–1731 (2013).
61. J. M. Winter, B. Joureau, E. J. Lee, B. Kiss, M. Yuen, V. A. Gupta, C. T. Pappas, C. C. Gregorio, G. J. Stienen, S. Edvardson, C. Wallgren-Pettersson, V. L. Lehtokari, K. Pelin, E. Malfatti, N. B. Romero, B. G. Engelen, N. C. Voermans, S. Donkervoort, C. G. Bönnemann, N. F. Clarke, A. H. Beggs, H. Granzier, C. A. Ottenheijm, Mutation-specific effects on thin filament length in thin filament myopathy. *Ann. Neurol.* **79**, 959–969 (2016).
62. E.-J. Lee, J. M. De Winter, D. Buck, J. R. Jasper, F. I. Malik, S. Labeit, C. A. Ottenheijm, H. Granzier, Fast skeletal muscle troponin activation increases force of mouse fast skeletal muscle and ameliorates weakness due to nebulin-deficiency. *PLOS ONE* **8**, e55861 (2013).
63. A. V. Hill, A. Hill, A. Paganini-Hill, The possible effects of the aggregation of the molecules of haemoglobin on its dissociation curves. *J. Physiol.* **40**, 4–7 (1910).
64. J. S. Walker, X. Li, P. M. Buttrick, Analysing force-pCa curves. *J. Muscle Res. Cell Motil.* **31**, 59–69 (2010).
65. B. Joureau, J. M. de Winter, S. Conijn, S. J. P. Bogaards, I. Kovacevic, A. Kalganov, M. Persson, J. Lindqvist, G. J. M. Stienen, T. C. Irving, W. Ma, M. Yuen, N. F. Clarke, D. E. Rassier, E. Malfatti, N. B. Romero, A. H. Beggs, C. A. C. Ottenheijm, Dysfunctional sarcomere contractility contributes to muscle weakness in ACTA1-related nemaline myopathy (NEM3). *Ann. Neurol.* **83**, 269–282 (2018).

66. C. A. Ottenheijm, C. C. Witt, G. J. Stienen, S. Labeit, A. H. Beggs, H. Granzier, Thin filament length dysregulation contributes to muscle weakness in nemaline myopathy patients with nebulin deficiency. *Hum. Mol. Genet.* **18**, 2359–2369 (2009).
67. S. Richards, N. Aziz, S. Bale, D. Bick, S. Das, J. Gastier-Foster, W. W. Grody, M. Hegde, E. Lyon, E. Spector, K. Voelkerding, H. L. Rehm; ACMG Laboratory Quality Assurance Committee, Standards and guidelines for the interpretation of sequence variants: A joint consensus recommendation of the American College of Medical Genetics and Genomics and the Association for Molecular Pathology. *Genet. Med.* **17**, 405–424 (2015).

Acknowledgments: We thank the families for participating in this study. We also would like to thank C. Mendoza (NINDS/NNDCS), G. Averion (NINDS/NNDCS), and K. Brooks (CTU/NINDS) for help in supporting the clinical research activities. We also thank the NIH Intramural Sequencing Center for performing the exome sequencing. This work was promoted within the European Reference Network (ERN) for Rare Neuromuscular Diseases. We thank the Associazione Centro Dino Ferrari for support. **Funding:** This work was supported by ZonMW-VICI grant (91819613 to C.A.C.O.) and ZonMW-VENI grant (09150161910168 to J.M.d.W.); intramural funds by the NINDS/NIH (to C.G.B.); Maximizing Investigators' Research Award (MIRA) (R35) from the National Institute of General Medical Sciences (NIGMS) of the National Institutes of Health (NIH), (R35GM124977 to P.M.K.-H.); Common Fund of the Office of the Director of the National Institutes of Health; by NCI, NHGRI, NHLBI, NIDA, NIMH, and NINDS to the Genotype-Tissue Expression (GTEx) Project; Italian Ministry of Health–IRCCS Ca' Granda Ospedale Maggiore Policlinico and SEQMD project (IRCCS Cà Granda Ospedale Maggiore Policlinico to G.P.C.); Australian National Health and Medical Research Council (NHMRC) Investigator Grant (APP2007769 to G.R.); NHMRC Ideas Grant (APP2002640 to G.R. and N.G.L.); National Institutes of Health and by American Physiological Society John F. Perkins Jr. Research

Career Enhancement Award (R01HL130318 to L.F.F.); "Multiplex Ligation-dependent Probe Amplification (MLPA) approach as a rapid and sensitive molecular tool for diagnosis and prognosis of Spinal Muscular Atrophy (SMA)" (11010168 to National Research Centre); and in-kind contribution of Monash University (to R.J.B.-R.). **Author contributions:** Conceptualization: S.D., M.v.d.L., G.R., N.G.L., P.M.K.-H., G.P.C., T.M., C.G.B., and C.A.C.O. Clinical and histological investigation: J.R., R.O., O.L.A.N., C.A.M., A.N.V., A.R.F., J.H.P., S.M., S.Z., S.B.N., L.M., L.N., N.A., T.M., F.M., and M.Z. Experiments and analyses: J.M.d.W., S.C., S.G., V.B., Y.H., K.I., S.M., M.R.D., P.M.K.-H., D.R., N.A., R.J.B.-R., L.B.M., D.H., L.F.F., K.R.J., Y.Z., W.S.-E., M.E., N.E., D.T.H., J.J.H., and F.I.M. Supervision: G.P.C., P.M.K.-H., C.G.B., and C.A.C.O. Writing—original draft: S.D., M.v.d.L., P.M.K.-H., C.G.B., and C.A.C.O. All authors reviewed and approved the manuscript. **Competing interests:** J.J.H., D.T.H., and F.I.M. are employees of Cytokinetics and were financially compensated for their work. The other authors declare that they have no competing interests. **Data and materials availability:** All data associated with this study are present in the paper or the Supplementary Materials. Patient-related data, including genetic sequencing data, were generated as part of the clinical diagnostic work-up. RNA sequencing data are available in SRA database (PRJNA1082398). Requests for deidentified patient data by academic investigators will be handled by the respective institutions and may be shared through a data transfer agreement. Select patient samples are available from C.G.B. under a material transfer agreement with the National Institute of Neurological Disorders and Stroke/ National Institutes of Health.

Submitted 23 May 2023

Accepted 11 March 2024

Published 3 April 2024

10.1126/scitranslmed.adg2841